

Arctic Sea Ice Volume Changes in Terms of Age as Revealed From Satellite Observations

Haibo Bi , Jinlun Zhang, Yunhe Wang, Zehua Zhang, Yi Zhang, Min Fu, Haijun Huang, and Xiuli Xu

Abstract—Satellite remote sensing provides new insight into the large-scale changes within the Arctic sea ice cover. In this study, satellite-derived sea ice parameters (thickness and age) were explored to investigate age-dependent Arctic sea ice volume changes. Between 2003–2008 (ICESat) and 2011–2015 (CryoSat-2), Arctic Ocean sea ice experienced a net depletion of roughly $4.68 \times 10^3 \text{ km}^3$ during autumn (October–November) and about 87% (or $4.11 \times 10^3 \text{ km}^3$) is caused by the removal in multiyear ice (two years and older). In spring (February–March), the net ice depletion amounts to $1.46 \times 10^3 \text{ km}^3$, with the multiyear ice loss of $3.74 \times 10^3 \text{ km}^3$ and seasonal ice increment of $2.24 \times 10^3 \text{ km}^3$. Among multiyear ice loss, about 74% (autumn) and 93% (spring) of the loss were attributable to the depletion of the oldest ice type (5 years and older). Analyses also affirm that the marvelous volume loss of multiyear ice during cold months (October–May) in 2006/2007 and 2011/2012, along with the low replenishment of perennial ice as noted in the following autumns in 2007 and 2012, plays a major role in leading to a younger Arctic sea ice cover. Consequently, these processes together favors for the overall substantial volume loss observed in the Arctic sea ice cover.

Index Terms—Age-dependent volume, arctic, remote sensing.

I. INTRODUCTION

ARCTIC sea ice stands out as one of the most visible components corresponding to climate changes. Recent dramatic decline in the summer ice extent are among the most obvious and drastic changes in the Arctic sea ice cover [1]–[4]. Other intriguing indicators include a decrease of multiyear ice [5]–[7], increases in drift speed [8], [9] and ice deformation rate [10], a basin-wide thinning of the ice cover [11]–[17], and substantial ice volume loss [12], [18]–[20]. In order to extract information about Arctic Ocean sea ice volume, sea ice thickness retrieved

from satellite measurements is of particular interest. Unlike sea ice extent, sea ice thickness retrieved from remote measurements has always been a great challenge.

Kwok and Cunningham [21] examined the trends and variability of sea ice volume using the five-year (2003–2008) ICESat-derived sea ice thickness. Tilling *et al.* [22] investigated the short-term (2010–2015) variability of Arctic sea ice volume using CS2-derived ice thickness, and a large sea ice volume variability was identified. Laxon *et al.* [20] explored the combined ICESat (2003–2008) and CS2 (2010–2012) record to investigate the inter-satellite Arctic sea ice volume changes, and substantial volume depletions by 4291 km^3 (autumn, October–November) and 1479 km^3 (spring, February–March) between the 2003–2008 and 2010–2012 periods was demonstrated. Moreover, Kwok and Cunningham [21] analyzed the changes of sea ice volumes with ICESat (2003–2008) data and extended records of CS2 (2010–2014), further confirming a marked decline in total Arctic sea ice volume estimates between the two satellite periods. Taken together, the near decadal record depicts losses in Arctic Ocean ice volume of $4170 \text{ km}^3/\text{decade}$ and $7760 \text{ km}^3/\text{decade}$ in winter (February–March, FM) and autumn (October–November, ON) [21].

Satellite-derived sea ice age is a record determined using ice motion data, and tracking how long older sea ice survives during the summer melt season in the Arctic Ocean. It has been used in two aspects: 1) identification between first year ice (FYI) and multiyear ice (MYI) and estimate of sea ice age of MYI; 2) as a proxy of thickness according to the established relationship between age and thickness. Based on sea ice age, changing age/thickness relationship and varying coverage in FYI and MYI has been well documented. In this study, we perform a further analysis of relating sea ice extent and volume changes to ice age, as multiple facts point to a rapid transition in the Arctic Ocean toward younger and thinner sea ice components.

Previous studies have examined the inter-satellite sea ice volume changes by treating the Arctic ice as an ensemble [20], [21]. However, little is known on how the sea ice volumes of different ages have been varying, given the clear trends towards younger and thinner components within the Arctic sea ice regime [6], [7]. Since older MYI ice is assumed to be thicker than younger ice [23], [24], the changes in age distribution should also imply for a net volume loss. By quantifying the sea ice volume changes in terms of ages, this study attempt to clarify the fundamental change in the nature of the sea ice volume balance within Arctic itself.

This study is organized as follows. Section II describes the datasets and methods. Section III presents changes of Arctic sea

Manuscript received January 31, 2017; revised June 30, 2017, December 15, 2017, and March 12, 2018; accepted April 3, 2018. This work was supported by the National Natural Science Foundation of China under Grant 41406215; Fund by Laboratory for Marine Geology, Qingdao National Laboratory for Marine Science and Technology, Postdoctoral Science Foundation of China under Grant 2014M561971. (Corresponding author: Haibo Bi.)

H. Bi, Z. Zhang, Y. Zhang, and H. Huang are with the Key Laboratory of Marine Geology and Environment, Institute of Oceanology, Chinese Academy of Sciences, Qingdao 266071, China (e-mail: bbb@qdio.ac.cn; zzh@qdio.ac.cn; 7706465@163.com; hjhuang@qdio.ac.cn).

J. Zhang is with the Applied Physics Laboratory, University of Washington, Seattle, WA 98195 USA (e-mail: zhang@apl.washington.edu).

Y. Wang is with the Marine Remote Sensing, Institute of Oceanology, Chinese Academy of Sciences, Qingdao 266071, China (e-mail: yhw1118@yeah.net).

M. Fu is with the Polar Science, National Marine Environmental Forecasting Center, Beijing 100081, China (e-mail: fum@nmefc.gov.cn).

X. Xu is with the First Institute of Oceanography, State Oceanic Administration (SOA), Qingdao 266061, China (e-mail: xuxiuli129@126.com).

Color versions of one or more of the figures in this paper are available online at <http://ieeexplore.ieee.org>.

Digital Object Identifier 10.1109/JSTARS.2018.2823735

1939-1404 © 2018 IEEE. Personal use is permitted, but republication/redistribution requires IEEE permission.

See http://www.ieee.org/publications_standards/publications/rights/index.html for more information.

ice volume associated with ice age between the two satellite periods (ICESat: 2003–2008, CS2: 2011–2015). Assessments of the satellite-derived ice thickness fields associated with ice ages are also outlined. Section IV discusses the results from the view of ice replenishment and depletion. Conclusion remarks are given in Section V.

II. DATA AND METHOD

A. ICESat and CS2 Sea Ice Thickness

Sea ice thickness fields are derived from ICESat and CS2 ice freeboard measurements. ICESat is the first satellite allowing the northernmost Arctic sea ice freeboard measurements up to 86°N , compared to 81.6°N by Envisat. The spatial coverage of polar sea ice freeboard observations is further expanded by the CS2 platforms which extends the northernmost latitudinal scope of observations up to 88°N .

ICESat and CS2 probe the earth surface with different types of sensor. The laser altimeter system onboard ICESat [25], [26] measures the freeboard height of the snow top, while the radar altimeter onboard CS2 operating at a much longer wavelength collects signals from the snow-ice interface [27], [28]. Following Archimedes principle, sea ice thickness can be retrieved from ice freeboards measured by ICESat [26], [29] and CS2 [20], [21] instruments following (1) and (2), respectively:

$$h_i = \frac{\rho_w}{\rho_w - \rho_i} f_b - \frac{\rho_w - \rho_s}{\rho_w - \rho_i} h_s \quad (1)$$

$$h_i = \frac{\rho_w}{\rho_w - \rho_i} f_b + \frac{\rho_s}{\rho_w - \rho_i} h_s \quad (2)$$

where h_i is the ice thickness, f_b the satellite-measured freeboard, h_s the snow depth, and ρ_w , ρ_i , and ρ_s correspond to the densities of water, ice, and snow, respectively. The ICESat and CS2-derived sea ice thickness has been provided by the Jet Propulsion Laboratory (JPL) in the National Aeronautics and Space Administration (NASA). Later, we briefly introduce input parameters used by JPL to derive sea ice thickness from ICESat and CS2 measurements.

For sea water and sea ice density terms, similar values (1025 and 917 kg/m^3) are used in the two satellite-based thickness retrievals [12], [21]. It is clear there should be a dependence of ρ_i on ice type. However, different parameterization methods of ρ_i as a function of thickness or ice type is difficult to reconcile and detailed information about sea ice density of different age or type seems lacking. Here, to ensure the comparability between ice volume of different satellite periods, we simply adopted the CS2-based thickness derived from the one fixed density of ρ_i , which is consistent with the use of ice density in the ICESat-derived sea ice thickness provided by JPL.

Large-scale observations about snow depth (h_s) and density (ρ_s) are sparse. In order to retrieve Arctic-wide sea ice thickness from ICESat data, JPL used meteorological snow depth derived from ECMWF fields [12] and modified snow density based on *in situ* measurements [32]. Assessments prove an overall good agreement (within bias of 0.1 m and uncertainty of 0.42 m) between the ICESat-retrieved ice thickness and *in situ* measurements from a submarine cruise in November 2005 [11]. Moreover, an overall mean bias of $0.1(\pm 0.51)\text{ m}$ is determined by

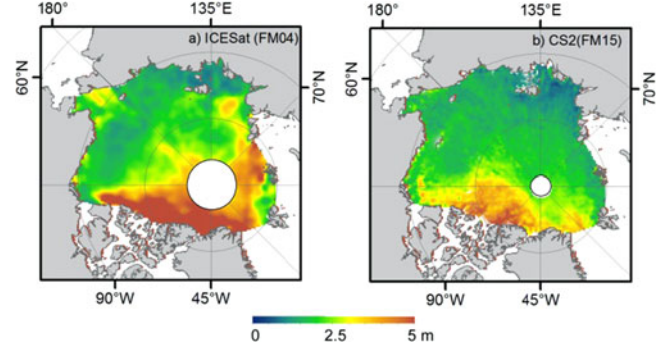


Fig. 1. Sea ice thickness derived from (a) ICESat and (b) CS2 measurements during February to March (FM) period in 2004 and 2015, respectively. There are data gaps of approximately 0.5 and $0.08 \times 10^6\text{ km}^2$ around the north pole for ICESat and CS2 observations. Retrievals out of the Arctic basin are cut off due to the inadequate knowledge about snow depth (Personal Communication with R. Kwok).

comparing ICESat retrievals with upward-looking sonar (ULS) measurements from Beaufort Gyre Exploration Project (BGEF) moorings. Numbers after \pm is the standard deviation of the differences.

CS2-derived sea ice thickness is obtained by JPL using climatology data of snow depth h_s and density ρ_s provided in Warren *et al.* [32] (hereafter W99). However, snow load uncertainty is a significant error source in the thickness retrievals and the application of snow depth and density on two satellite observations should be consistent. Therefore, as used in the retrieval of ice thickness using ICESat freeboard, in this study sea ice thickness based on CS2 measurements is recalculated with snow depth from ECMWF fields and snow density from [32]. The sea ice thickness retrievals are then evaluated with respect to its age (see Fig. 6 in Section III). To avoid the problem of ‘too thick’ snow on thin ice, an effective snow depth (ESD) term is used following [32]. The ESD is taken to be a fraction of total freeboard as defined by a sigmoidal curve [32]. For example, when the total freeboard is half of the snow depth, the total freeboard is divided to $1/3$ ice freeboard and $2/3$ snow height. The ECMWF-derived snow depth get the entire effect only when ratio of total freeboard and snow depth is no less than 1.3 [32]. This treatment, to a certain degree, fixes the problem of snow depth overestimation due to local freeboard variability associated with snow loss to new openings as well as unmodeled redistribution of snow mass.

Both ICESat- and CS2-derived sea ice thickness fields used here are available on a 25 km grid. Samples of the two satellite-derived ice thickness are given in Fig. 1. The ICESat observations of spanning roughly one-month are available in October–November (ON) and February–March (FM)/March–April (MA) periods between 2003 and 2008 [12]. For CS2, the monthly sea ice thickness during cold seasons (October through May) for the 2011–2015 period are available [21].

B. Ice Concentration and Sea Ice Age

Sea ice concentration (SIC) is obtained from the National Snow and Ice Data Center (NSIDC) [38]. The NSIDC product is derived by applying the NASA Team algorithm to bright temperatures acquired by satellite passive microwave

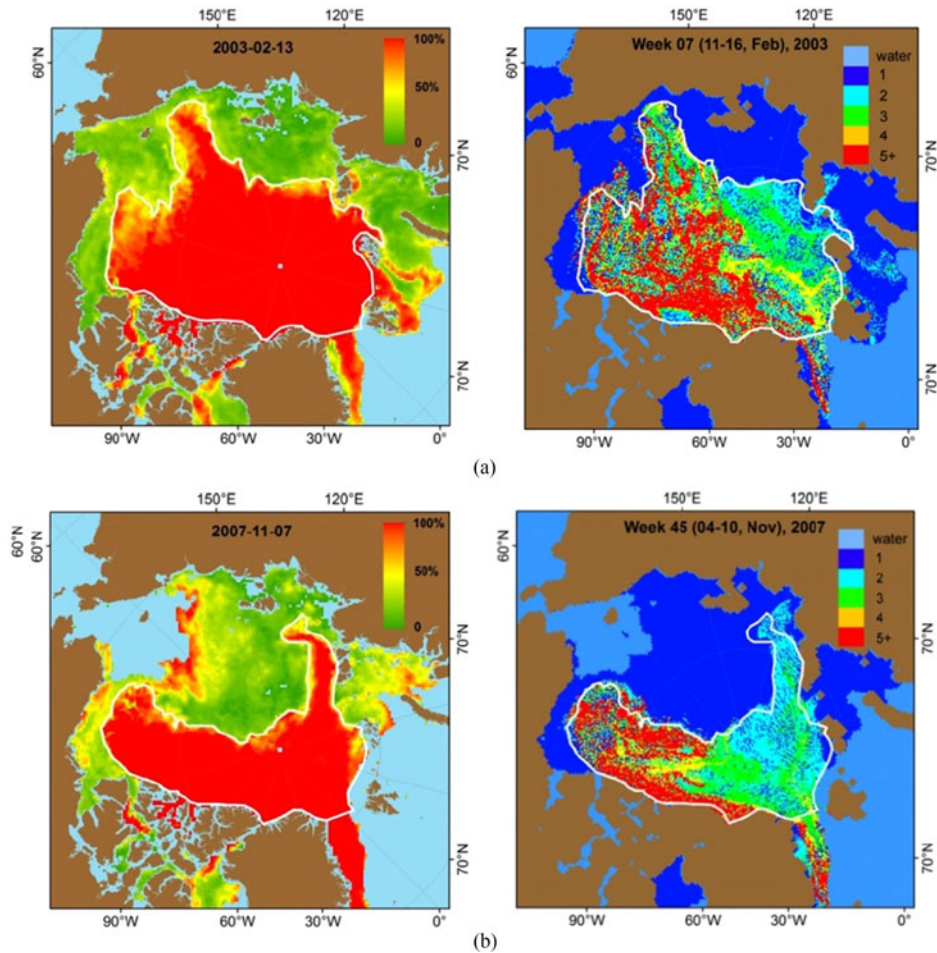


Fig. 2. Comparisons between spatial distributions of MYI extent. (a) and (c) Derived from QuikSCAT measurements. (b) and (d) Derived from NSIDC age product. The samples in February 2003 and November 2007 are selected at random. The white solid lines superimposed on maps refer to the 50% contour line of the QuikSCAT-derived MYI ice concentrations [43].

(PMW) radiometry. The SIC record covers a long time series (1978.11–2015.05), and has a grid resolution of 25 km.

Sea ice age [39] available at NSIDC is derived from sea ice motion [40]. Tracking ice motion, sea ice age is determined by treating an individual grid that contains ice as an independent Lagrangian particle, which were transported at weekly time steps following ice motion trajectories at 12.5 km spatial resolution in Equal Area Scalable Earth (EASE) grid. The motion vectors are derived using a cross-correlation technique applied to sequential, daily satellite images acquired by Scanning Scanning Multichannel Microwave Radiometer (SMMR), the Special Sensor Microwave Imager (SSM/I), the SSM/I Sounder (SSMIS), and the Advanced Microwave Scanning Radiometer–Earth Observing System (AMSR-E) sensors. Then, these vectors are optimally blended with drifting-buoy vectors from the International Arctic Buoy Program (IABP) and wind vectors deduced from NCEP/NCAR Reanalysis. Daily sea ice motion product are available in NSIDC.

The sea ice age product is built on NSIDC sea ice motion product. Theoretically, if a seasonal ice particle survives the summer melt, then it should be considered to have aged for one year, or an additional year in the case of multiyear ice. Since

ice parcels are independently tracked, merging or diverging with the neighboring parcels may happen. Therefore, the ice age in each grid cell denotes the oldest parcel of that grid. Sea ice assigned as one year old is actually at most one year old, an ice age of two years is between one and two years old, and so on. The age data spans 1979 to present and the first six years are considered as a spin-up period for the model initialization. Therefore, the sea ice age product exactly starts from 1985.

Sources of uncertainty for sea ice age product originate from two aspects: 1) tracking error associated with the spatial resolution of coarse 25 km drift motion; and 2) land-masking uncertainties related to the dismissing of ice motion near the coast [24]. Additionally, uncertainties may be caused by the mechanisms dealing with the converging and diverging cases. For instance, if two or more parcels converge into a grid, only the oldest age is saved for that grid. This may produce a larger coverage for older ice [24]. On the contrary, if no MYI parcel is present in a grid cell, but the ice extent indicates that ice exists there (i.e., diverge case occurs), that ice is considered FYI [24]. The divergence-related fill-up by FYI are common within the MYI ice pack (see Fig. 2). However, a recent report pointed out that the some divergence may be unrealistic and associated

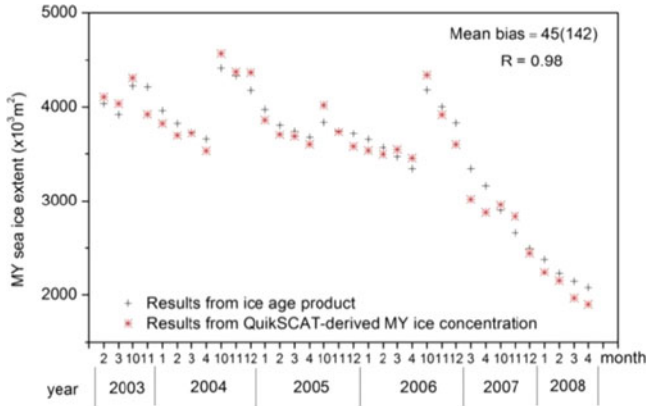


Fig. 3. Comparison between MYI extent derived from NSIDC ice age product (black cross) and QuikSCAT retrievals (red asterisk). Monthly estimates of cold seasons (October to May) between 2003 and 2008 are shown. Correlation (R), mean, and standard deviation of difference are also given (inset texts).

with the faster drifts in places where the blending of buoy drifts introduces a faster ice advection relative to neighboring sea ice motion retrieved from satellite observations [42].

Sea ice motion product has a higher accuracy when using higher spatial resolution satellite imagery. For example SSMIS imagery from 37 GHz channel (25 km with oversampled resolution) can provide daily motions with a root-mean-square (rms) accuracy of 6–7 km/day, while the 91 GHz channel on SSMIS can provide daily motions with an rms accuracy of 4–5 km/day. The application of an optimal interpolation scheme allows the gridded fields show an uncertainty of 3–4 km/day. The fairly high daily RMS errors are further reduced after averaging these uncorrelated daily vectors into weekly estimates. Assessed with ERS-1 synthetic aperture radar (SAR) data, the ice motion product results in an error of about 0.9 to 1.6 km/day. The daily RMS error in the ice motion product is not necessarily cumulative since the annual displacement errors are found on the order of 50–100 km.

The effectiveness of sea ice age data in separating multiyear ice (MYI) from first-year ice (FYI) has been examined by comparing with QuikSCAT retrievals [41]. Fig. 2 shows the the spatial distribution patterns of samples for MYI extents respectively derived from QuikSCAT and ice age data. Fig. 3 presents the time series between 2003 and 2008 with respect to the monthly MYI extents derived from the two products, which agrees well with a mean bias of approximately $44.8 (\pm 142.8) \times 10^3 \text{ km}^2$.

C. Sea Ice Volume in Terms of Sea Ice Age

Arctic sea ice volume is estimated within the Arctic Ocean bounded by the openings into peripheral oceans: Bering Strait into the Pacific, Fram Strait and Barents Seas into the North Atlantic. The surveyed area covers an area of approximately 7.2 million km^2 (see Fig. 4). In common with ICESat-derived thickness fields, age-dependent sea ice volume between 2003 and 2008 are obtained during autumn (ON) and spring (FM) periods. Corresponding period of ice volume (average volume of October and November for ON; average of February and March for FM) are computed over the CS2 case (2011–2015).

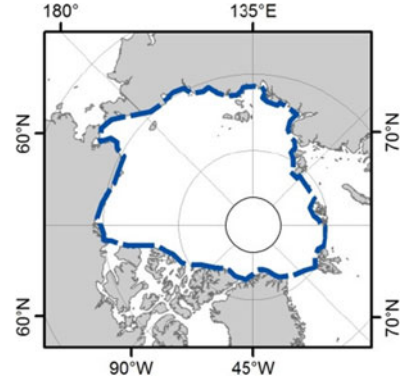


Fig. 4. Boundary of the surveyed area to compute sea ice volume.

For consistency the two satellite-based sea ice volume estimate do exclude ice cover north of 86°N due to the observational hole of ICESat. For sea ice age data, we selected the weeks in the mid-period of ON (or FM) as the representative age distributions for autumn (or spring).

Ice volume within a grid cell is calculated as the product of the three parameters: sea ice thickness (h_i), ice concentration (c_i), and area ($A = 156.25 \text{ km}^2$) of that grid. To determine age-related volume, satellite-derived sea ice thickness and concentrations should be co-registered with age fields. The thickness and concentration record are re-gridded and averaged to the 12.5 km EASE grid of ice age product.

The original sea ice age has a range from 1 up to 10 years. In this study, we binned the ice of 5 years and older to the 5+ category in that numbers of ice grids older more than 6 years are much less. Following (3), we are able to determine the sea ice volume (V_s) of cell grids ($i = 1, 2, 3, \dots, n$) with an age of s ($s = 1, 2, 3, \dots, 5+$)

$$V_s = A \sum_{i=1}^n c_i h_i. \quad (3)$$

The uncertainty in total ice volume (σ_V) can be computed as follows:

$$\sigma_V = A \left[\sum_{i=1}^n (h_i^2 \sigma_{c,i}^2 + c_i^2 \sigma_{h,i}^2) + \sigma_{\text{age},i}^2 \right]^{1/2} \quad (4)$$

where $\sigma_{h,i}$ and $\sigma_{c,i}$ represent the uncertainties in thickness and ice concentration, respectively, at the cell grid suffixed as i . n is the total number of grid cells for ice with a specific age s within the surveyed Arctic Ocean. For the uncertainty of concentration ($\sigma_{c,i}$), we choose a typical value of 5% since it is generally low during freezing seasons when high concentrations are popular [44].

Annual ice parcel displacement error based on the NSIDC ice motion product shows a upper bound RMS error of 100 km. Accordingly, thickness/volume uncertainty due to sea ice age error (σ_{age}) [see Fig. 5(b)] is here defined as the standard deviation of thickness/volume differences between the estimates of the grids and those surrounding the center grid within 100 km in radius, roughly corresponding to a 5×5 grid pattern with respect to the ICESat or CS2 EASE grid of 25 km.

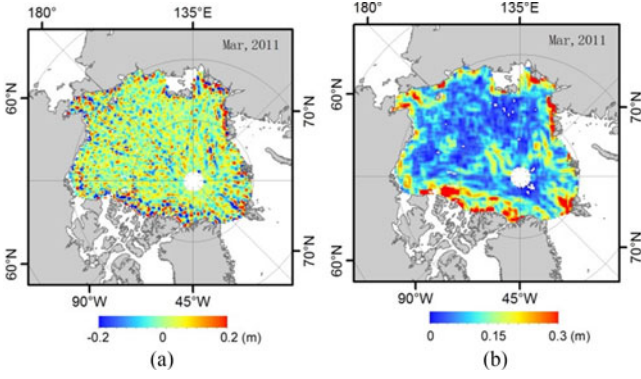


Fig. 5. Sea ice thickness (a) bias and (b) uncertainty due to uncertainty of sea ice age error caused by NSIDC ice motion misplacement.

For the uncertainty of the ice thickness ($\sigma_{h,i}$), it is associated with five variables (f_b , h_s , ρ_w , ρ_i , and ρ_s) as shown in (5). The error of the ice thickness $\sigma_{h,i}$, calculated by Gaussian error propagation from the input variables and their errors, is deduced as [29]

$$\begin{aligned} \sigma_{h_i}^2 = & \sigma_{f_b}^2 \left(\frac{\partial h_i}{\partial f_b} \right)^2 + \sigma_{f_b}^2 \left(\frac{\partial h_i}{\partial h_s} \right)^2 + \sigma_{\rho_s}^2 \left(\frac{\partial h_i}{\partial \rho_s} \right)^2 \\ & + \sigma_{\rho_i}^2 \left(\frac{\partial h_i}{\partial \rho_i} \right)^2 + \sigma_{\rho_w}^2 \left(\frac{\partial h_i}{\partial \rho_w} \right)^2 \end{aligned} \quad (5)$$

where

$$\begin{aligned} \frac{\partial h_i}{\partial f_b} &= \frac{\rho_w}{\rho_w - \rho_i} \\ \frac{\partial h_i}{\partial h_s} &= -\frac{\rho_w - \rho_s}{\rho_w - \rho_i} (\text{ICESat}) \text{ or } \frac{\rho_s}{\rho_w - \rho_i} (\text{CS2}) \\ \frac{\partial h_i}{\partial \rho_s} &= \frac{h_s}{\rho_w - \rho_i} \\ \frac{\partial h_i}{\partial \rho_i} &= -\frac{h_i}{\rho_w - \rho_i} \\ \frac{\partial h_i}{\partial \rho_w} &= \frac{-\rho_i f_b + (\rho_i - \rho_s) h_s}{(\rho_w - \rho_i)^2} (\text{ICESat}) \frac{\rho_i f_b + \rho_s h_s}{-(\rho_w - \rho_i)^2} (\text{CS2}). \end{aligned}$$

The representative values for the errors in input variables are summarized in Table I.

D. Ancillary Data

Ice draft and thickness data from varying platforms are used to assess the satellite-derived products (ICESat and CS2). These include measurements from the following: 1) a submarine surveying transect of approximately 3 km in length crossing the Arctic basin; 2) three to four moorings of the Beaufort Gyre Exploration Project (BGEF); and 3) aircraft campaigns of the Operation IceBridge (OIB) program. The positions or tracks for these datasets are presented in Fig. 6 in the following section.

The submarine data were collected in November 2005 and digitalized from [12], which represent the mean drafts for segments of the cruise varying from 5 to 50 km in length. The draft data are expected to be biased 29 cm and a

variability of 25 cm compared to actual draft because of the first return nature of the echoes. The bias has been removed before use [12]. Ice drafts from BGEF are obtained with moored upward looking sonars (ULS) deployed in the Canada Basin (www.who.edu/beaufortgyre). The moorings have been in operation since 2003. The sonars measure the range to the sea ice bottom surface every two seconds and have a footprint about 2 m. For the ICEat period (2003–2008), data from four moorings [see Fig. 6(a)] are utilized, while for recent CS2 period (2011–2015) only three instruments remain available [see Fig. 5(b)]. Methods used to process and calibrate sonar measurements to yield ice draft are described in [47]. Typically, individual ice drafts are accurate by an order of within ± 0.1 m (95% confidence limits).

Ice thickness from OIB is derived from lidar-measured (the Airborne Topographic Mapper) ice freeboard (ice plus snow) and radar-measured snow depth. It has a nominal 1 m resolution with about 200 m swath and is averaged to give a mean for 40 m segments of the flight line. In other words, each data point in longitude/latitude represents a 40 m \times 200 m area [24]. The uncertainties are variable, depending on the determination of sea surface and quality of snow depth [48]. The OIB campaign survey tracks cover the major part of the western Arctic between northern Greenland and Alaska [see Fig. 5(b)]. The data from five OIB missions during March and April from 2011 to 2015 are used [48], [49]. Wherein the IceBridge Sea Ice Freeboard, Snow Depth, and Thickness (L4 Version 1) dataset (2011–2013) is obtained from the National Snow and Ice Data Center (NSIDC) and the relevant methods to retrieve ice thickness is described in [46] and [47]. The remaining OIB data for the time span 2014–2015 is a quick-look product, also archived at NSIDC [50]. These data may assume more uncertainty in comparison with the OIB L4 data for 2009–2013 [49]. Before the use of these data, they are resampled into the 12.5 km EASE grid of sea ice age data using a drop-into-bucket method [24].

III. RESULTS

A. Assessments of Satellite-Derived Sea Ice Thickness in Terms of Ice Age

To provide a preliminary estimate about the bias and uncertainty in Arctic sea ice volume estimates, satellite-derived sea ice thickness fields of different ages are evaluated with *in situ* and/or aircraft measurements spanning different spatial scales. Fig. 6 shows the locations and tracks of the data used to assess the satellite retrievals. The vast coverage of these data could provide a relatively good descriptive statistics of the accuracy with respect to the age-dependent sea ice thickness. Comparative results are shown in Fig. 7. The acquired bias and uncertainty terms (given as the inset texts in Fig. 7) are further employed to estimate the sea ice volume errors (see Section III-D).

ICESat-derived drafts (ice thickness below the sea surface, i.e., draft = thickness – freeboard) for sea ice of different ages manifest a distinct difference compared to submarine records ranging from -0.18 m (one year) to 0.42 m (two years) [see Fig. 7(a)]. Generally, low correlations are also found between them, which is partially caused by the limited numbers of data

TABLE I
TYPICAL VALUES AND UNCERTAINTIES FOR INPUT VARIABLES USED TO COMPUTE THE UNCERTAINTY OF THICKNESS ESTIMATES FROM ICESAT
AND CS2 MEASUREMENTS

Variables	Values	Uncertainty	Reference
ice density (ρ_i , kg/m ³)	920	ON/FM: 15	[45]
Snow density (ρ_s , kg/m ³)	Monthly variables	ON:80; FM: 60	[46]
Sea water density (ρ_w , kg/m ³)	1025	ON/FM: 0.5	[20, 29]
Ice concentration (e)	NASA Team	ON/FM: 0.08	[44]
Snow depth (s , m)	Meteorological fields from ECMWF	ON/FM: 0.10	[21]
Freeboard (f_b , m)	ICESat/CS2	0.14	[14, 41]

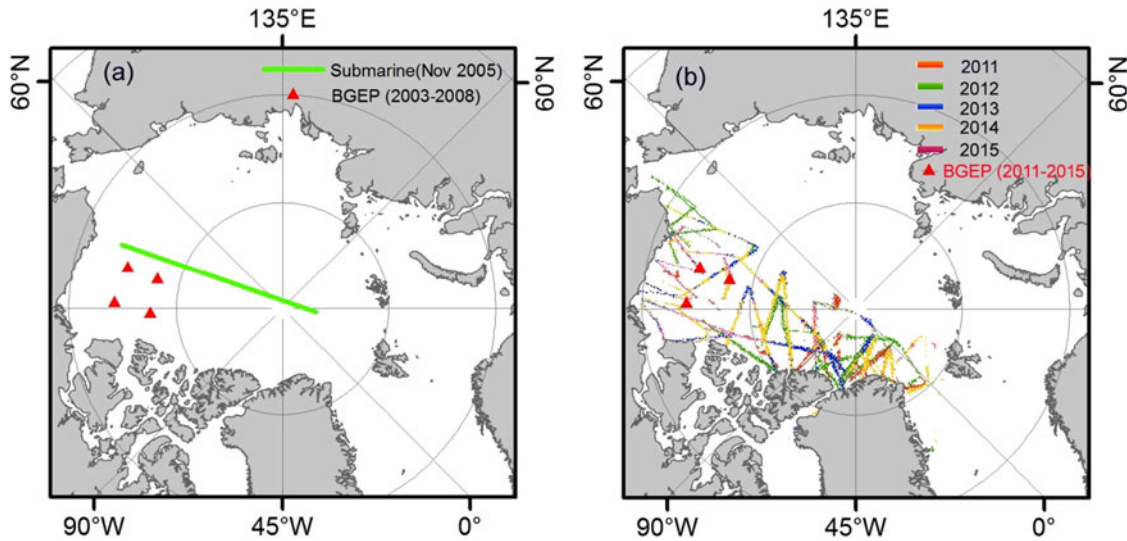


Fig. 6. Locations and track for data used to evaluate satellite-derived sea ice thickness during a) ICESat period (2003–2008) and b) CS2 period (2011–2015). BGEF moorings are marked as red triangles; the submarine track in November 2015 is indicated by the green line; the OIB footprints are represented with different colors.

available in the comparison. The differences between ICESat-derived drafts and BGEF ULS mooring observations span a range from -0.3 m (four years) to 0.07 m (five years), and the correlations are significant at least in the 90% confidence level [see Fig. 7(b)].

CS2 sea ice thickness basically overestimates the ULS and OIB measurements [see Fig. 7(c) and (d)]. The biases between CS2 and ULS data cover a range of between 0.05 m (one year) and 0.22 m (5+ years), with statistically significant correlations of generally (except for 5+ ice) exceeding the 99% confidence level [see Fig. 7(c)]. Differences between CS2 and OIB thickness estimates vary from 0.11 m (one year) and 0.30 m (three years), and statistically significant correlations exceeding the 99% level are identified despite of age variations.

The relatively large standard deviations, as shown by quantities included in parentheses in the inset texts in Fig. 7, are suggestive of a noticeable variability of differences between satellite-derived ice thickness and *in situ* measurements, which

are in part caused by the inconsistency in temporal and spatial scales between different data sources.

The feasibility of adapted snow depth climatology (W99) [32] to retrieve CS2 sea ice thickness has been broadly demonstrated [51]–[53]. According to [53], there is a mean difference of 0.004 m (with a standard deviation of difference (st.d) of 0.66 m, and a correlation of 0.67) for W99-based CS2 ice thickness and Icebridge data for the spring between 2011 and 2014. This is much smaller than the difference achieved in this study of 0.21 m but comparable to our evaluation in the sense of st.d (0.63 m) and correlation (0.65). Note that there exists a great deal of Icebridge footprints quite near to the coast of northern Canadian Archipelago, where CS2 freeboard may be prone to be overestimated due to the mixing effect from stronger land echoes [54]. After the elimination of co-located grids which is close to the coastline less than 25 km (the use of 50 km threshold, which corresponds to the size of two CS2 grid cells, could masked out the grids that may be contaminated by land speckle

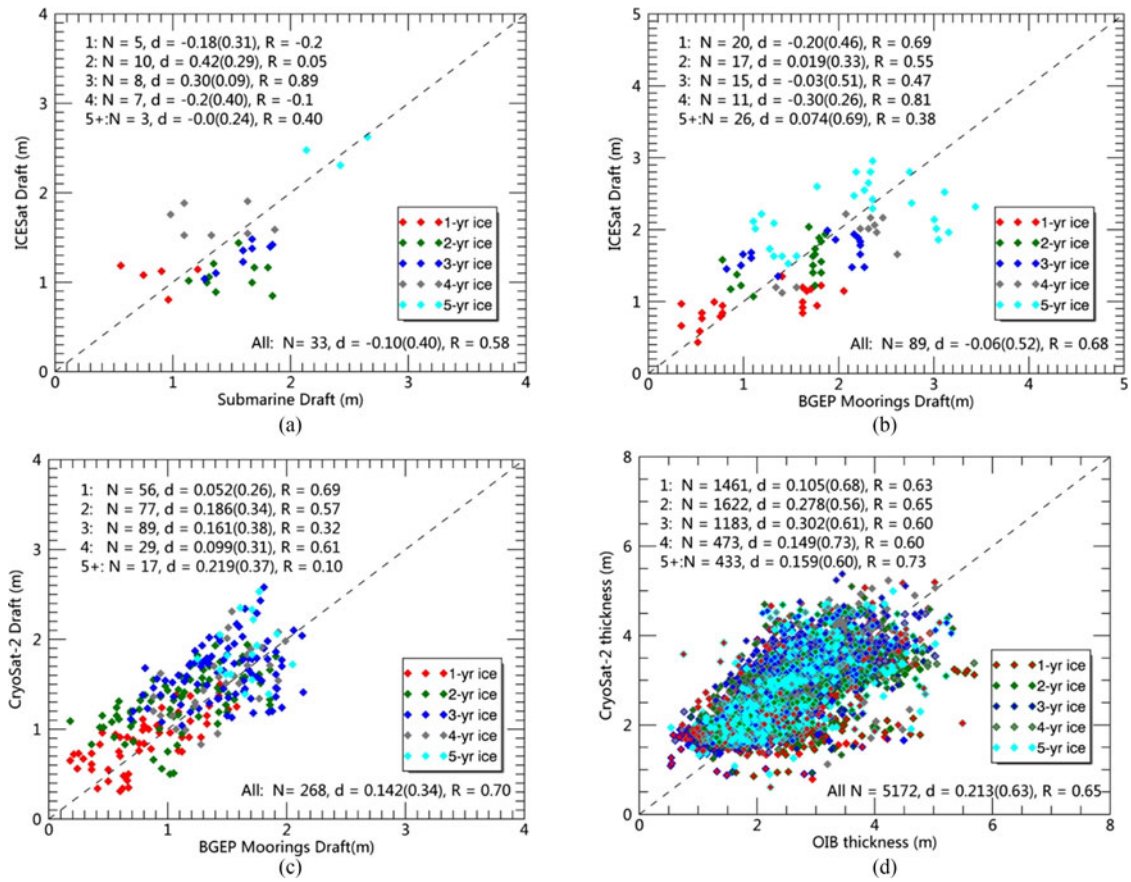


Fig. 7. Assessments of satellite-derived sea ice thickness/draft of different ages. Comparison of ICESat-derived drafts. (a) With a submarine. (b) With BGEP mooring data. CS2 estimates are compared. (c) To BGEP mooring observations. (d) To OIB measurements. N is the number of data available in the comparison, d is the mean difference (unit: m) and numbers in the parentheses denote the standard deviation of difference, and R corresponds to the correlation coefficient.

noise and could keep as much valid data points as possible), the overall difference between our CS2-derived thickness and Icebridge data is reduced to 0.08 m (with st.d of 0.64 m and correlation of 0.68). In addition, Tilling *et al.* [46] obtained the difference between sea ice volume based on sea ice thickness using adapted W99 snow depth and Reanalysis product for the Amerasian and Eurasian basins. They found that the two results are slightly different from each other, with a difference of less than 5%. Similarly, we also found a good agreement between the two kinds of results (i.e., sea ice volume derived from CS2 thickness using W99 snow depth versus that based on Reanalysis snow product) for the same basins, with a high correlation of 0.98 and a difference no more than 7% (see Fig. 8).

B. Spatiotemporal Distribution Patterns of Sea Ice Age During the Two Satellite Periods

For a visual presentation about the changes within the Arctic sea ice pack, the spatial distribution of sea ice age fields for autumn and spring months over ICESat and CS2 periods are provided (see Figs. 9 and 10). Dramatic changes were clear in the west Arctic Ocean, where the major part of the old ice (5+ ice) that was distinct in ICESat period (see Fig. 9) has almost completely depleted in CS2 period (see Fig. 10). A close examination about the loss of 5+ ice from the sea ice age time

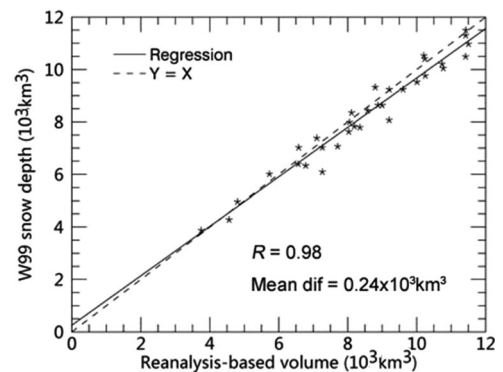


Fig. 8. Comparison between CS2-based sea ice volume estimates using snow depth derived from Reanalysis snow depth and W99 snow climatology data.

series between 2009 and 2010 period (not shown) suggests that the oldest ice has been melted out during the following summer months in Beaufort and Chukchi Seas where ice dynamics is typically driven by the Beaufort Gyre (BG) system. As a response, younger ice replaced the older ice, was pushed against northern Canadian Archipelago and Greenland, and currently dominates the west Arctic (see Fig. 10). Since the younger ice occupies more area in the present Arctic Ocean, the vulnerability of sea ice to summer melting should be enhanced. In fact,

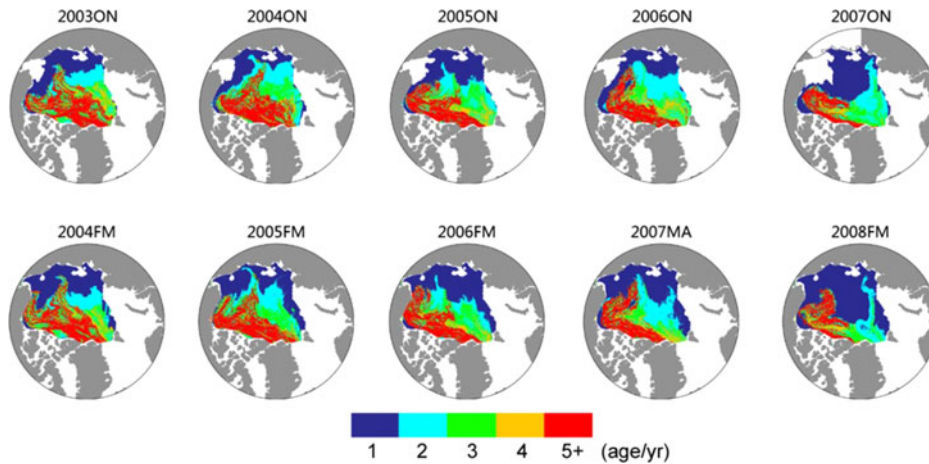


Fig. 9. Sea ice age distribution during autumn (October to November, ON) and spring (February to March or March to April, FM or MA) periods over 2003–2008 (ICESat period).

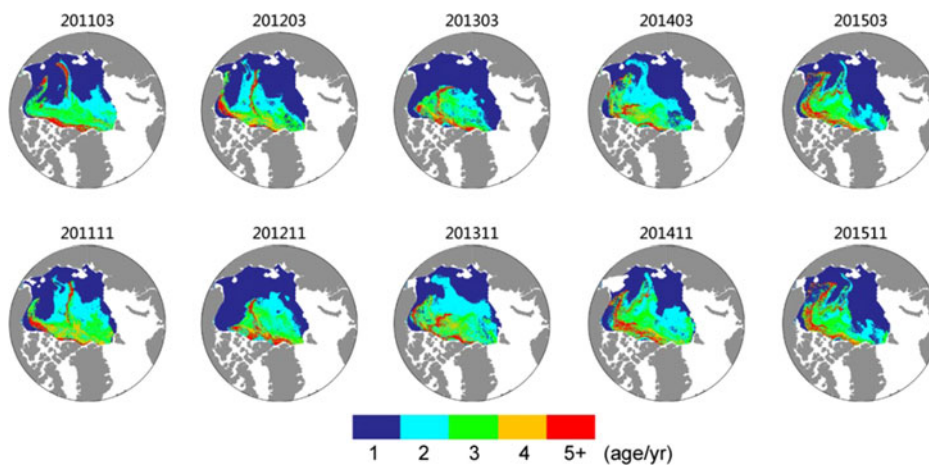


Fig. 10. Sea ice age components for the autumn (November) and spring (March) periods over 2011–2015 (CS2 period).

during the ICESat period the summer melting (FYI coverage as suggested by the ON maps in Fig. 9) was mostly confined in the southern marginal seas (except for 2007). By contrast, during recent CS2 period, the melting extent (FYI extent as indicated in the November maps in Fig. 10) was escalated into areas of further north and substantial removal of MYI cover are observed in the November maps of 2014 and 2015.

The faster sea ice drifting speed, reinforced by the replacement of older and thicker ice by younger and thinner components [8]–[10], allows ice to be transported more rapidly toward the southern peripheral seas (such as Beaufort and Chukchi Seas) where substantial ice melt may occur. Therefore, the survivability of old ice seems to be generally low as reflected in the maps during CS2 period (see Fig. 10). The alternation in sea ice constitutes within the Arctic preconditions for a large volume changes of old sea ice.

C. Arctic Sea Cover Changes Between 2003–2008 and 2011–2015

To discern the Arctic Ocean age-dependent sea ice changes, the combined record of ICESat (2003–2008) and

CS2 (2011–2015) measurements are analyzed. ICESat record is generally available in autumn (ON) and spring (FM) periods. For inter-satellite consistency, the averaged thickness estimates of the two months (October and November) from CS2 record is used as the proxy of autumn record (ON) and the averaged value of Feb and Mar is selected to represent the spring record (FM). Figs. 10–12 show the obtained age-dependent sea ice thickness, area, and volume, respectively, in autumn (blue lines) and spring (red lines) over the two satellite periods.

Between the two periods, sea ice thickness of all ages showed a decrease in both seasons (see Table II and Fig. 11). The ice thickness with respect to the entire Arctic sea ice cover, on average, has declined by 0.96 m (ON) and 0.73 m (FM) [see Table II and Fig. 10(a)]. The thickness decreases for MYI cover (two years and older) during both seasons are larger than those of FYI, 1.08 versus 0.48 m in autumn (ON) and 0.73 versus 0.52 m in spring (FM) (see Fig. 10(b) and (g) and Table II). Within MYI pack, the oldest type [see 5+ ice in Fig. 11(g)] reduced the most, by 1.5 m in ON and 0.9 m in FM. An increased trend for sea ice thickness reduction, as ice aged, appeared in autumn (see Table II). This approves that porous older MYI ice is more sensitive to the amplified warming impacts in Arctic.

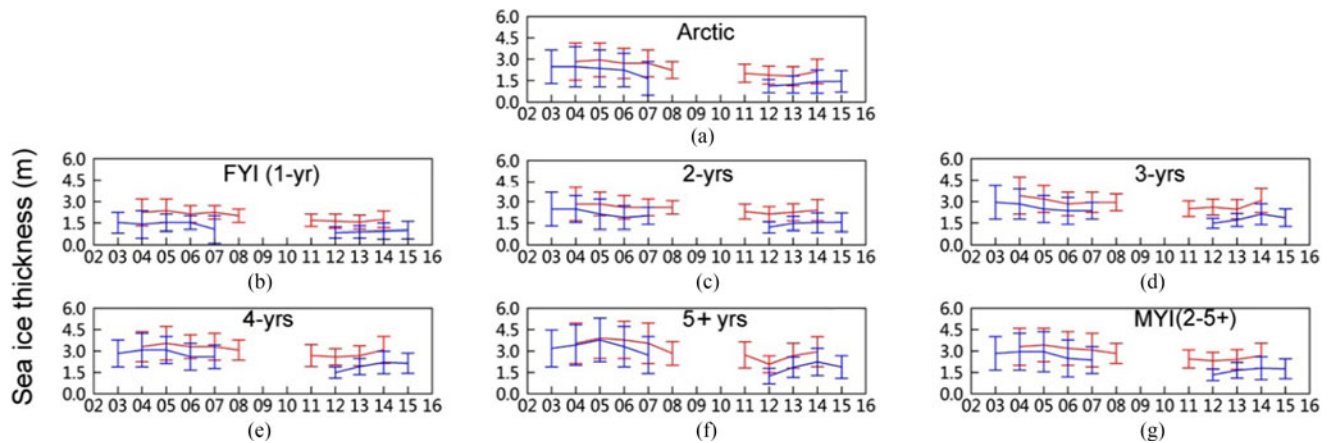


Fig. 11. Average sea ice thickness of different ages for autumn (blue) and spring (red) records over the 2003–2008 (ICESat) and 2011–2015 (CS2) periods. (a) Overall Arctic sea ice. (b) One year. (c) Two years. (d) Three years. (e) Four years. (f) 5+ years. (g) MYI: two years and older. Error bars represent the standard deviation of ice thickness (x unit: period from 2002 to 2016, and y unit: m).

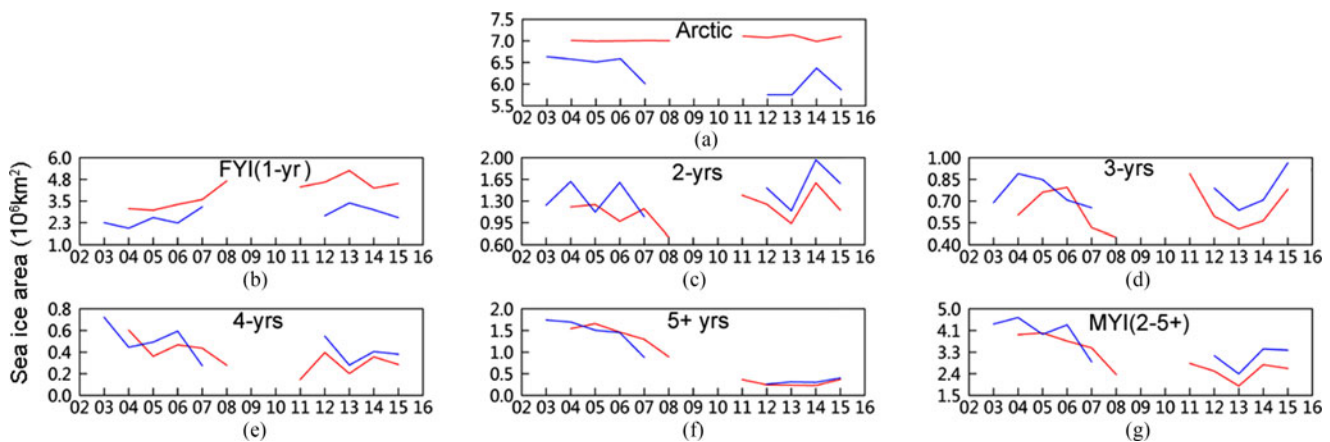


Fig. 12. As with Fig. 11 but for sea ice area (x unit: period from 2002 to 2016, and y unit: 10^6 km^2).

TABLE II

MEAN VALUES OF SEA ICE AREA, SEA ICE VOLUME, THICKNESS FOR DIFFERENT ICE AGES OVER THE AUTUMN (ON) AND SPRING (FM) SEASONS DURING THE TWO SATELLITE PERIODS (THE CORRESPONDING AUTUMN (ON) AND SPRING (FM) DIFFERENCES BETWEEN THE TWO SATELLITE PERIODS ARE ALSO GIVEN)

	Satellites	Periods	1yr	2yr	3yr	4yr	5+yr	2-5+yr	All ages
Ice area (10^6 km^2)	ICESat	ON	2.42	1.32	0.76	0.51	1.46	4.04	6.47
		FM	3.51	1.06	0.63	0.43	1.37	3.49	7.00
	CS2	ON	2.89	1.55	0.77	0.40	0.32	3.05	5.93
		FM	4.58	1.26	0.67	0.28	0.29	2.44	7.08
	Difference	ON	0.47*	0.23	0.01	-0.11	-1.14*	-0.99*	-0.54*
		FM	1.07*	0.20	0.04	-0.15	-1.08*	-1.05*	0.08
Volume (10^3 km^3)	ICESat	ON	2.85	2.46	1.65	1.20	4.09	9.42	12.26
		FM	6.46	2.40	1.61	1.20	4.17	4.51	15.84
	CS2	ON	3.06	2.04	1.26	0.69	0.53	9.38	7.58
		FM	8.70	2.65	1.62	0.72	0.69	5.68	14.38
	Difference	ON	0.22	-0.43	0.39*	-0.51*	-3.56*	-4.90*	-4.68*
		FM	2.24*	0.25	-0.02	-0.49*	-3.48*	-3.70*	-1.46*
Thickness (m)	ICESat	ON	1.42	2.19	2.55	2.78	3.28	2.71	2.24
		FM	2.19	2.67	3.02	3.30	3.51	3.16	2.69
	CS2	ON	0.93	1.44	1.80	1.93	1.83	1.63	1.28
		FM	1.67	2.30	2.69	2.82	2.63	2.50	1.96
	Difference	ON	-0.48*	-0.75*	-0.75*	-0.85*	-1.48*	-1.08*	-0.96*
		FM	-0.52*	-0.37*	-0.33*	-0.48*	-0.88*	-0.67*	-0.73*

Note: *mark the differences that are larger than one standard deviation of the means of both the ICESat and the CS2 records.

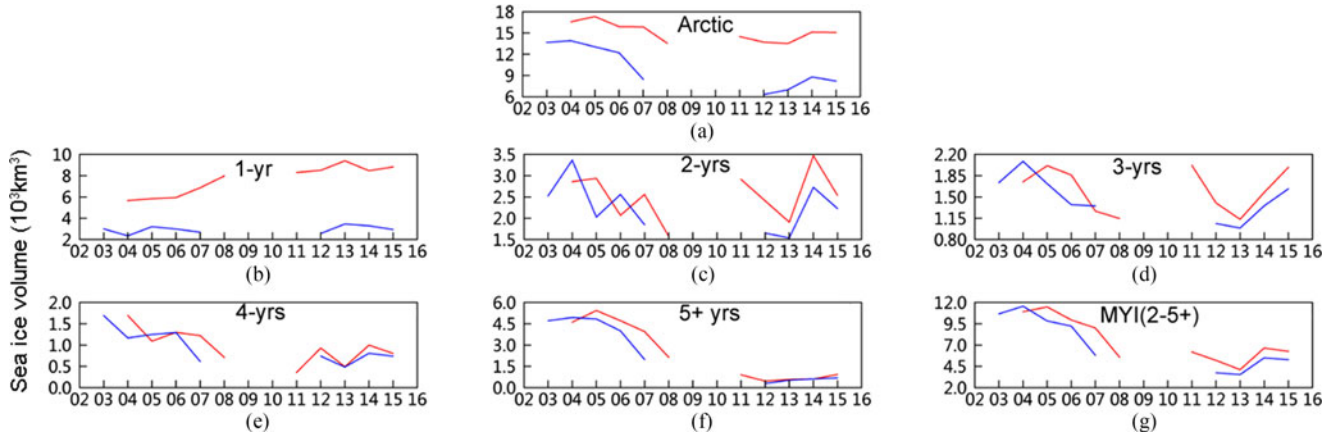


Fig. 13. As with Fig. 12 but for sea ice volume (x unit: period from 2002 to 2016, and y unit: 10^3 km^3).

The large standard deviations for thickness (see Fig. 11) imply for a greater regional variability due to dynamic and thermodynamic forcing acting on it. Meanwhile, smaller thickness declines of about 0.3 m on average across MYI pack (two years and older) was detected in PIOMAS simulations [23].

Fig. 11 corroborates the facts that sea ice thickness decreases is more significant during autumn than spring between the two satellite periods [20], [21]. The delayed autumn freeze-up due to the dramatic summer ice loss, commonly observed during the past decade, is in part responsible for the distinguished thickness decline through all ice elements [55]. The spring (FM) thickness decrease between the two satellite periods is not such evident, in that the thinner ice generally grow faster when the freezing period gets started. All these scenarios pave a way for the dramatic Arctic sea ice volume loss.

The changes of total Arctic sea ice area is different depending on seasons. A clear decrease ($0.52 \times 10^6 \text{ km}^2$) in Arctic sea ice coverage is observed for autumn record between 2003–2008 and 2011–2015, while it remains almost unchanged in spring [see Fig. 12(a)]. The increases in FYI coverage of $0.47 \times 10^6 \text{ km}^2$ (autumn) and $1.07 \times 10^6 \text{ km}^2$ (spring) are remarkable [see Table II and Fig. 10(b)]. On the contrary, MYI cover has been experiencing large and comparable decreases in autumn ($0.99 \times 10^6 \text{ km}^2$) and spring ($1.05 \times 10^6 \text{ km}^2$) between the two periods [see Table II and Fig. 12(g)]. Within MYI pack, the major component contributing to the large retreat of perennial ice cover is the oldest ice type [i.e., 5+ ice, Fig. 11(f)], with the average decreases of 1.14 and $1.08 \times 10^6 \text{ km}^2$ during autumn and spring periods, respectively (see Table II). Also, we found a decrease for ice four years ice (see Fig. 10(e) and Table II). By contrast, the younger MYI cover (two and three years ice) went through slight increases between the two periods [see Fig. 12(c) and (d)]. These facts are in agreement with other studies [6], [7] arguing that the Arctic sea ice cover is becoming younger and thinner.

Due to changes in the spatial distribution of sea ice, sea ice volume changes between the two periods are astonishing. The entire Arctic Ocean sea ice cover presented a volume reduction of $4.68 \times 10^3 \text{ km}^3$ (autumn, from 12.26 to $7.58 \times 10^3 \text{ km}^3$) and $1.46 \times 10^3 \text{ km}^3$ (spring, from 15.84 to $13.84 \times 10^3 \text{ km}^3$)

(see Table II). In terms of percentage, these correspond to 37% (ON) and 9% (FM) of the mean estimates of ICESat periods (2003–2008). These changes are comparable to the calculation in [20] for the ICESat (2003–2008) and CS2 (2010–2012) periods, by 4291 km^3 (ON) and 1479 km^3 (FM).

The near decadal record, taken ICESat and CS2 together, shows the Arctic sea ice volume loss rate of $4050 \text{ km}^3/\text{decade}$ in autumn (ON) and $7200 \text{ km}^3/\text{decade}$ in spring (FM), comparable to estimates in [21] of $7760 \text{ km}^3/\text{decade}$ and $4170 \text{ km}^3/\text{decade}$ using CS2 record for 2010–2014. Our estimates represent a much slower trend compared to those obtained during the ICESat period, $8620 \text{ km}^3/\text{decade}$ (FM) and $12370 \text{ km}^3/\text{decade}$ (ON) [12]. The overall decelerated trend is chiefly caused by the ice volume recovery during the later CS2 period, particularly obvious in 2014 and 2015 [see Fig. 13(a)].

Apparently, the increase in FYI volume only counteract a small part of the volume loss due to the markedly depletion of MYI [see Fig. 13(b) and (g)]. The average FYI volume increased by $0.22 \times 10^3 \text{ km}^3$ (autumn) and $2.24 \times 10^3 \text{ km}^3$ (spring) (see Table II). Meanwhile, MYI volume reduced by $4.90 \times 10^3 \text{ km}^3$ (autumn) and $3.70 \times 10^3 \text{ km}^3$ (spring) (see Table II).

Within MYI, the largest loss of approximately $3.5 \times 10^3 \text{ km}^3$ in both seasons is observed for the oldest ice types (i.e., 5+ ice) (see Fig. 12(f) and Table II). There is also a decrease in four years ice by about $0.5 \times 10^3 \text{ km}^3$ for both seasons [see Fig. 13(e)]. For the younger MYI ice (two and three years ice), the changes in volume were complicated (see Fig. 13(c) and (d) and Table II) because of the compensation effects due to increase or decrease in area and thickness. Table II also suggests that the net large volume loss in Arctic sea ice for both seasons between the two satellite periods is largely controlled by the significant decline in thickness and extreme shrinkage in area of ice four years and older.

D. Error Estimate in Ice Volume

Following [21], the volume errors (e_{vol}) can be defined as a simple form as follows:

$$e_{\text{vol}}(s) = A_s(e_h + e_a) \pm \sigma_{v_s} \quad (6)$$

TABLE III
SYSTEMATIC BIAS IN ARCTIC SEA ICE VOLUME ESTIMATES (UNIT: 10^3 km^3)

	1	2	3	4	5+	MYI	Total
ICESat ^a	-0.27	0.02	-0.01	-0.12	-0.10	-0.21	-0.48
ICESat ^b	-0.43	0.52	0.24	-0.10	-0.01	0.65	0.22
CS2 ^c	0.21	0.22	0.11	0.03	0.06	0.42	0.63
CS2 ^d	0.42	0.32	0.20	0.03	0.05	0.6	1.02

Note: ^{a,b,c,d} represent volume bias estimated with sample error in satellite-derived thickness that is evaluated with submarine (2015), ULS (2003-2008), ULS(2011-2015), and OIB (2011-2015) data, respectively (Figure 6).

where e_h is the systematic bias between satellite-derived thickness and evaluation data, e_a is the mean bias [see Fig. 5(a)] of thickness due to sea ice age error caused by NSIDC ice motion displacement error and defined as the bias between thickness of the center grid and those of the neighboring 5×5 grids (grids within a radius of 100 km of the center grid); A_s is the total area for ice with an age of s ; $\sigma_{v,s}$ is the uncertainty estimate of ice volume calculated with (2)–(6). The comparison between satellite-derived ice thickness and available measurements from aircraft and *in situ* campaigns were used to provide sample values of the bias term (e_h). Employing the sample mean bias in Figs. 5 and 7, the bias in age-dependent volume is computed as $A_s(e_h + e_a)$ (assuming the bias distribution is spatially homogeneous) and results are listed in Table III.

The bias term in volume error is different as evaluation data varies (see Table III). Total Arctic sea ice volume are biased of -530 km^3 (ULS) and 230 km^3 (Submarine) for ICESat-based estimates. CS2-derived ice volume are biased about 660 km^3 (ULS) and 1120 km^3 (OIB). Table III also suggests that the bias over CS2 period seems to be larger for younger ice (one to three years ice) and smaller for older ice (four years and older) compared to those for ICESat, consistent with the fact that younger ice currently is taking for more coverage in the Arctic Ocean. On average, the ice volume bias of different ages (see Table III, -430 to 520 km^3) generally amount to less than 9% of the corresponding mean ice volume estimates (see Table II) over the corresponding periods.

According to the uncertainty ($\sigma_{v,s}$) due to the significant error sources in the input parameters as listed in Table I, we arrived the combined error estimates in a root-sum-square manner [46]. The uncertainties are 183 – 626 km^3 (ON) and 160 – 865 km^3 (FM) (depending on ice ages) for the 2003–2008 period, and on the ranges of 105 – 468 km^3 (ON) and 92 – 1165 km^3 (FM) for the 2011–2015 period. The Arctic Ocean sea ice volume uncertainties for CS2 period amount to 12.2% (FM) and 15.3% (ON) of the mean sea ice volume estimates for different ages in different seasons. These errors are comparable to the uncertainties presented in [46], which is 13.0% and 14.5% for Arctic sea ice volume in April and October, respectively.

It is also necessary to analyze the inter-satellite bias before examining the sea ice volume changes between the two satellite periods. However, a qualified test is currently unpractical due to the lack of well-assessed representative common dataset with sufficient spatial and temporal overlapping with the two satellite observations. Our assessments based on ULS data indicate

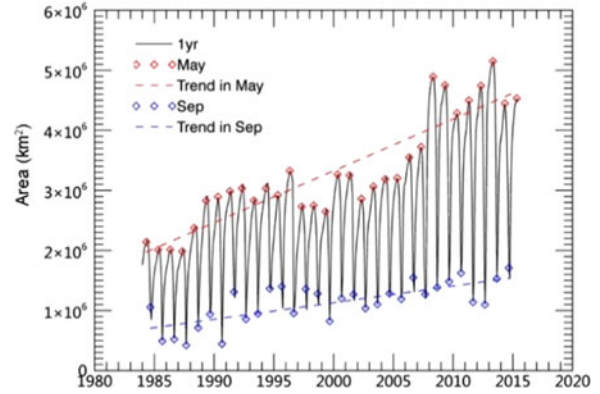


Fig. 14. Monthly FYI coverage over the period 1984–2015. The records in May (annual maximum) and in Sep (annual minimum) are marked as red and blue diamonds, respectively. The trends for May and September are also given (red and blue dashed lines).

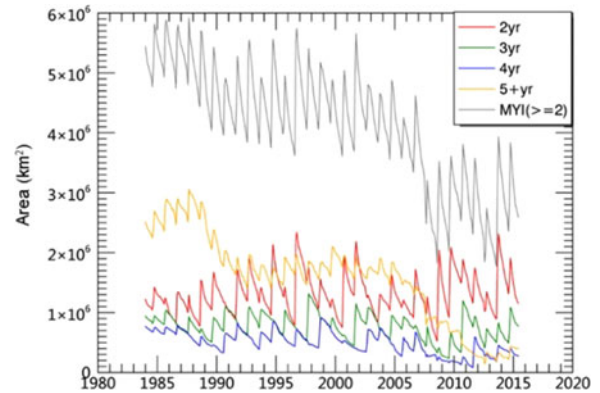


Fig. 15. As Fig. 14 but for all kinds of ice with varying ages.

an intersatellite bias of 0.2 m for ICESat (-0.06 m) and CS2 (0.14 m), roughly representing an intersatellite difference of approximately 1350 km^3 in total Arctic ice volume estimates. This difference is comparable in magnitude to our estimates of spring (FM) ice volume decrease of 1460 km^3 between two satellite periods, but unmatched to the decline in autumn (ON) of 4680 km^3 .

IV. DISCUSSION

To better understand the large loss in volume between two satellite periods, we placed the past decadal ice component changes under a long-term background. The monthly area time series for FYI and MYI (determined from ice age) between 1984 and 2015 are presented in Figs. 14 and 15, respectively.

Fig. 14 outlines an increasingly enlarged seasonal cycle in FYI area time series, which is mainly associated with the larger positive trend of FYI area in May. It is easy to interpret that there would be more FYI in winter owing to increased MYI loss in coverage to be replaced by newly produced FYI. Also, it is interesting to note that the Arctic sea ice cover contained more FYI ice in Sep during recent decade compared to 1980s. Therefore, the Arctic sea ice is currently more prone to suffer from large summer melting processes. It has been pointed out that the nine record low ice extents in September has occurred

for the past nine years before 2015 [56]. Marked disappearance of bright ice in summer allows the dark ocean to absorb more solar radiation and heat up. This would, in a positive feedback way, enhance the lateral and bottom melting of sea ice. Moreover, absorbed energy by ocean can delay the timing of autumn sea water freeze-up and thus shorten the period of ice growth [55]. The outcome of the substantial Arctic sea ice depletion in summer is thus translated into the decreases in ice thickness and volume during cold seasons, which is obvious in our comparison between the two satellite periods.

The time series of MYI coverage of different ages is given in Fig. 15. During the mid- to late-1980s, the Arctic Ocean maintains in a stage of high MYI ice coverage. Afterward, it is kept in a relatively moderate level through the whole 1990s and early 2000s. Since mid-2000s, the MYI cover shows a trend of continued loss. It turns out that the anomalously low replenishment for MYI area in autumn of 2007 led to a new phase of low MYI [12]. Without any exceptionally large replenishment, the MYI ice loiters within a range of 2 to 4×10^6 km² after 2007. In addition, the record loss in MYI cover in summer 2012 is followed by a relative weak retreat during the following winter in 2012/2013 and a large recovery of MYI ice in autumn 2013, which prevents the MYI coverage from sliding to a new level of low coverage (see Fig. 15).

The overall trend of the MYI coverage is largely controlled by that of the oldest ice (5+ ice) which, in reference to area, is characteristic with three periods (high: 1984–1989, moderate: 1991–2005, low: 2012–2015) (see Fig. 15). The year-to-year area variability of the MYI ice is primarily attributable to the changes of the 2-year ice coverage (correlation $R = 0.83$).

Fig. 15 indicates a relatively stable annual replenishment of younger MYI for older ones. Indeed, the one-year delay correlation between 2 and 3 and 3 and 4 ice is relatively high ($R = 0.78$ and 0.75). However, the depletion of 5+ ice since 2008 indicates a reduced replenishment for ice of four years and beyond toward older ones, and the one-year delay correlation between 4 and 5+ ice is weak ($R = 0.5$). This mechanism favors for a transition toward younger ice components within the Arctic Ocean. Along with the distinct shrinkage of MYI coverage, the low survivability of the oldest MYI components foresees a reduced Arctic ice volume since mid-2000s.

To gain more sights about the changes in the Arctic Ocean sea ice cover from the view of replenishment, we estimate the annual production and depletion amounts in ice coverage for both FYI and MYI components between 1984 and 2015 (see Fig. 16). For FYI, it generally melts between May-Sep and grows from Sep through next May (see Fig. 14). Therefore, we referred the annual ice production and loss estimates in FYI zone as to the changes between May and Sep and between Sep and next May, respectively. For MYI, it usually is replenished from August (annual minimum) to October (annual maximum) and depletes from October to next August (see Fig. 15). Accordingly, the annual production and depletion estimates in MYI coverage are calculated as changes between August and October and between October and next August, respectively. The results are illustrated in Fig. 16.

Fig. 16 shows that the annual behavior of FYI area production (dashed red line) during cold seasons (September to May)

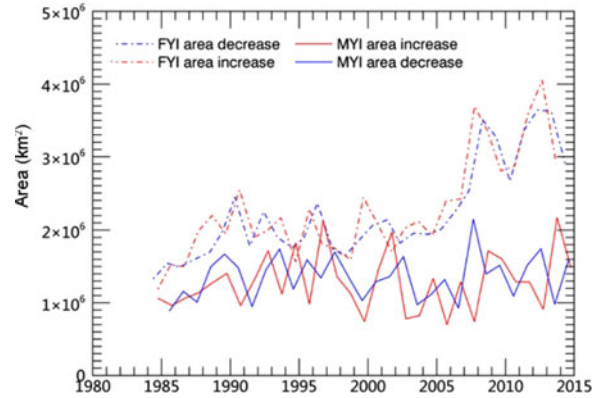


Fig. 16. Sea ice area generation (increase) and elimination (decrease) for FYI and MYI covers.

and depletion (dashed blue line) during following warm seasons (May to September) is in good agreement, with a mean difference of 1.2×10^3 km² and a correlation of 0.95. Furthermore, both the sea ice growth and loss in FYI zone underwent a similar positive trend (about 1.1×10^5 km²/year, statistically significant at 99%). Moreover, the recent (post-2007) annual winter growth and summer depletion in FYI component came through a sudden increases since 2008, amounting to 3×10^6 km², compared to those before 2007 (approximately 1.8×10^6 km²). To conclude, the replenishment/loss of FYI cover are basically maintained in a nearly balance status, which brings limited benefits to the overall recovery of perennial ice in the Arctic Ocean.

The annual variability is more complicated with regard to the replenishment and loss within MYI ice. Sea ice replenishment in autumn (solid red line in Fig. 16) and the loss in following melting seasons (solid blue line in Fig. 16) does not show any hint of a clear trend. The area balance for MYI cover is not held as good as for FYI. A moderate correlation of 0.65 is obtained between the time series of replenishment and loss in MYI ice coverage (solid lines in Fig. 16). Since 2005, there is a difference of -6×10^4 km², on average, between replenishment and loss, pointing to a net area loss in MYI zone. In particular, the extremely large MYI area retreat of about 2×10^6 km² in 2006/07 (October to August) is followed by the anomalously low (1×10^6 km²) replenishment of the MYI cover during the following autumn (2007) [12]. Consequently, a significant drop of MYI coverage between 2006 and 2008 emerged (see Fig. 14). Another significant shrinkage in MYI coverage (around 1.5×10^6 km²) was observed in 2011/2012 and followed by a low ice remedy in autumn of 2012 (roughly 1×10^6 km²) (see Figs. 15 and 16). These two anomalies are favorable for shifting the Arctic sea ice toward a younger and thinner components, facilitating a net volume loss within the MYI regime as demonstrated by preceding results [20], [21], which is also affirmed in our estimates based on satellite observations.

V. CONCLUSION

Based on satellite-derived retrievals, we obtain the sea ice volume estimates in terms of ice age over the two satellite

periods (ICESat: 2003–2008 and CS2: 2011–2015). Results point to a significant decline in overall Arctic sea ice volume, with more significant changes in autumn than in spring. The evident decreases in total ice volume between the two satellite periods are controlled by the changes in older ice components (five years and older). Furthermore, the variability and changes of sea ice are discussed from the standpoints of area balance. Analyses confirm that the unprecedented high MYI (two years and older) depletion during cold months (October to May) in 2006/2007 and 2011/2012, together with the anomalous low autumn replenishment in 2007 and 2012, contributes to the recent substantial decline in coverage of perennial ice. This serves to reformulate the Arctic sea ice cover toward younger constituents.

The decreased Arctic sea ice volume could trigger a broad environmental response. For instance, the significant sea ice volume loss is considered to have an important influence on the sea ice mass balance, ocean salinity anomaly, as well as fresh water cycles in the Arctic Ocean. In addition, heat and momentum exchanges are likely reinforced, in view of the vital role of sea ice as a blanket to modulate the energy flux between Arctic Ocean and air, which may augment the warming effect within and beyond the Arctic regimes.

Although the uncertainty for our ice volume estimates are small, the bias term is relatively large, about several percent relative to the total Arctic sea ice volume. Errors induced by ice thickness originate from multiple sources, such as different temporal and spatial scales of the data and acquisition and processing techniques between different satellite products. However, based on the current knowledge, it is hard to draw a more accurate quantitative conclusion about sea ice volume changes between the ICESat and CS2 periods. To fill this gap, more reliable knowledge of inter-satellite bias, derived from well overlapped independent measurements with a finer spatiotemporal coverage, is needed. The new instrument onboard the ICESat-2 to be launched in 2017 encourages such an opportunity.

ACKNOWLEDGMENT

The authors would like to thank R. Kwok in JPL for providing the ICESat and CS2 sea ice thickness data. Ice concentration and sea ice age data were archived at NSIDC. In addition, the authors would like to appreciate the anonymous reviewers for their insightful comments. They would like to thank the editors of the IEEE JSTARS for their suggestions. This work was performed at the Polar Science Center (PSC), Applied Physics Laboratory (APL), University of Washington (UW).

REFERENCES

- [1] C. L. Parkinson and J. C. Comiso, "On the 2012 record low Arctic sea ice cover: Combined impact of preconditioning and an August storm," *Geophys. Res. Lett.*, vol. 40, pp. 1356–1361, 2013.
- [2] S. T. Strey, W. L. Chapman, and J. E. Walsh, "The 2007 sea ice minimum: Impacts on the northern hemisphere atmosphere in late autumn and early winter," *J. Geophys. Res.: Atmos.*, vol. 115, pp. 6696–6705, 2010.
- [3] J. Stroeve *et al.*, "Arctic sea ice extent plummets in 2007," *Eos Trans. Amer. Geophys. Union*, vol. 89, pp. 13–14, 2008.
- [4] J. Zhang, R. Lindsay, A. Schweiger, and M. Steele, "The impact of an intense summer cyclone on 2012 Arctic sea ice retreat," *Geophys. Res. Lett.*, vol. 40, pp. 720–726, 2013.
- [5] J. C. Comiso, "Large decadal decline of the Arctic multiyear ice cover," *J. Clim.*, vol. 25, pp. 1176–1193, 2012.
- [6] J. Maslanik, J. Stroeve, C. Fowler, and W. Emery, "Distribution and trends in Arctic sea ice age through spring 2011," *Geophys. Res. Lett.*, vol. 38, pp. 392–392, 2011.
- [7] J. A. Maslanik *et al.*, "A younger, thinner Arctic ice cover: Increased potential for rapid, extensive sea-ice loss," *Geophys. Res. Lett.*, vol. 34, pp. 497–507, 2007.
- [8] R. Kwok, G. Spreen, and S. Pang, "Arctic sea ice circulation and drift speed: Decadal trends and ocean currents," *J. Geophys. Res.: Atmos.*, vol. 118, pp. 2408–2425, 2013.
- [9] G. Spreen, R. Kwok, and D. Menemenlis, "Trends in arctic sea ice drift and role of wind forcing: 1992–2009," *Geophys. Res. Lett.*, vol. 38, 2011, doi: [10.1029/2011GL048970](https://doi.org/10.1029/2011GL048970).
- [10] P. Rampal, J. Weiss, and D. Marsan, "Positive trend in the mean speed and deformation rate of Arctic sea ice, 1979–2007," *J. Geophys. Res.: Atmos.*, vol. 114, pp. 1289–1301, 2009.
- [11] E. Hansen *et al.*, "Thinning of Arctic sea ice observed in Fram Strait: 1990–2011," *J. Geophys. Res.: Oceans*, vol. 118, pp. 5202–5221, 2013.
- [12] R. Kwok, G. Cunningham, M. Wensnahan, I. Rigor, H. Zwally, and D. Yi, "Thinning and volume loss of the arctic Ocean sea ice cover: 2003–2008," *J. Geophys. Res.: Oceans*, vol. 114, pp. 371–377, 2009.
- [13] R. Kwok and D. Rothrock, "Decline in Arctic sea ice thickness from submarine and ICESat records: 1958–2008," *Geophys. Res. Lett.*, vol. 36, pp. 1985–2008, 2009.
- [14] A. H. H. Renner *et al.*, "Evidence of arctic sea ice thinning from direct observations," *Geophys. Res. Lett.*, vol. 41, pp. 5029–5036, 2014.
- [15] D. Rothrock, D. Percival, and M. Wensnahan, "The decline in arctic sea-ice thickness: Separating the spatial, annual, and interannual variability in a quarter century of submarine data," *J. Geophys. Res.: Oceans*, vol. 113, pp. 763–773, 2008.
- [16] Timmermans, "The impact of stored solar heat on Arctic sea ice growth," *Geophys. Res. Lett.*, vol. 42, pp. 6399–6406, 2015.
- [17] E. Hansen, S. Gerland, K. V. Høyland, O. Pavlova, and G. Spreen, "Time variability in the annual cycle of sea ice thickness in the transpolar drift," *J. Geophys. Res.: Oceans*, vol. 120, pp. 8135–8150, 2015.
- [18] S. Bathiany, D. Notz, T. Mauritsen, G. Raedel, and V. Brovkin, "On the potential for abrupt arctic winter sea ice loss," *J. Clim.*, vol. 29, pp. 2703–2719, 2016.
- [19] N. Kurtz *et al.*, "IceBridge airborne survey data support arctic sea ice predictions," *Eos Trans. Amer. Geophys. Union*, vol. 94, pp. 41–41, 2013.
- [20] S. W. Laxon *et al.*, "CryoSat-2 estimates of arctic sea ice thickness and volume," *Geophys. Res. Lett.*, vol. 40, pp. 732–737, 2013.
- [21] R. Kwok and G. F. Cunningham, "Variability of arctic sea ice thickness and volume from CryoSat-2," *Phil. Trans. R. Soc. A Math. Phys. Eng. Sci.*, vol. 373, 2015, doi: [10.1098/rsta.2014.0157](https://doi.org/10.1098/rsta.2014.0157).
- [22] R. L. Tilling, A. Ridout, A. Shepherd, and D. J. Wingham, "Increased Arctic sea ice volume after anomalously low melting in 2013," *Nat. Geosci.*, vol. 8, pp. 643–646, 2015.
- [23] H. Bi, M. Fu, K. Sun, Y. Liu, X. Xu, and H. Huang, "Arctic sea ice thickness changes in terms of sea ice age," *Acta Oceanol. Sin.*, vol. 35, pp. 1–10, 2016.
- [24] M. A. Tschudi, J. C. Stroeve, and J. S. Stewart, "Relating the age of Arctic sea ice to its thickness, as measured during NASA's ICESat and IceBridge campaigns," *Remote Sens.*, vol. 8, p. 457, 2016.
- [25] H. J. Zwally *et al.*, "ICESat's laser measurements of polar ice, atmosphere, ocean, and land," *J. Geodyn.*, vol. 34, pp. 405–445, 2002.
- [26] H. J. Zwally, D. Yi, R. Kwok, and Y. Zhao, "ICESat measurements of sea ice freeboard and estimates of sea ice thickness in the Weddell sea," *J. Geophys. Res.: Oceans*, vol. 113, pp. 228–236, 2008.
- [27] T. W. Armitage and M. W. Davidson, "Using the interferometric capabilities of the esa cryosat-2 mission to improve the accuracy of sea ice freeboard retrievals," *IEEE Trans. Geosci. Rem. Sens.*, vol. 52, pp. 529–536, 2014.
- [28] C. Gommenginger, C. Martin-Puig, S. Dinardo, D. Cotton, M. Srokosz, and J. Benveniste, "Improved altimetric accuracy of SAR altimeters over the ocean: Observational evidence from Cryosat-2 SAR and Jason-2," in *Proc. OSTST Meeting*, 2011, pp. 19–21.
- [29] R. Kwok and G. Cunningham, "ICESat over Arctic sea ice: Estimation of snow depth and ice thickness," *J. Geophys. Res.: Oceans*, vol. 113, pp. 179–185, 2008.
- [30] G. Spreen, S. Kern, D. Stammer, and E. Hansen, "Fram Strait sea ice volume export estimated between 2003 and 2008 from satellite data," *Geophys. Res. Lett.*, vol. 36, pp. 1–6, 2009.

- [31] H. Bi, H. Huang, Q. Su, L. Yan, Y. Liu, and X. Xu, "An Arctic sea ice thickness variability revealed from satellite altimetric measurements," *Acta Oceanol. Sin.*, vol. 33, pp. 134–140, 2014.
- [32] S. G. Warren *et al.*, "Snow depth on Arctic sea ice," *J. Clim.*, vol. 12, pp. 1814–1829, 1999.
- [33] T. W. K. Armitage and A. L. Ridout, "Arctic sea ice freeboard from AltiKa and comparison with CryoSat-2 and operation IceBridge," *Geophys. Res. Lett.*, vol. 42, pp. 6724–6731, 2015.
- [34] N. T. Kurtz, N. Galin, and M. Studinger, "An improved CryoSat-2 sea ice freeboard retrieval algorithm through the use of waveform fitting," *Cryosphere*, vol. 8, pp. 1217–1237, 2014.
- [35] R. Kwok, "Simulated effects of a snow layer on retrieval of CryoSat-2 sea ice freeboard," *Geophys. Res. Lett.*, vol. 41, pp. 5014–5020, 2014.
- [36] R. Ricker, S. Hendricks, D. K. Perovich, V. Helm, and R. Gerdes, "Impact of snow accumulation on CryoSat-2 range retrievals over arctic sea ice: An observational approach with buoy data," *Geophys. Res. Lett.*, vol. 42, pp. 4447–4455, 2015.
- [37] R. Lindsay and A. Schweiger, "Arctic sea ice thickness loss determined using subsurface, aircraft, and satellite observations," *Cryosphere*, vol. 9, pp. 269–283, 2015.
- [38] D. J. Cavalieri, C. L. Parkinson, P. Gloersen, and H. Zwally, Updated Yearly. Sea Ice Concentrations from Nimbus-7 SMMR and DMSP SSM/I-SSMIS Passive Microwave Data. Boulder, CO, USA: NASA National Snow and Ice Data Center Distributed Active Archive Center, 1996.
- [39] M. Tschudi, C. Fowler, J. Maslanik, J. S. Stewart, and W. Meier., *EASE-Grid Sea Ice Age, Version 3. Boulder, CO, USA: NASA National Snow and Ice Data Center Distributed Active Archive Center*, 2016, doi: [10.5067/PFSVFZA9Y85G](https://doi.org/10.5067/PFSVFZA9Y85G).
- [40] M. Tschudi, C. Fowler, J. Maslanik, J. S. Stewart, and W. Meier, *Polar Pathfinder Daily 25 km EASE-Grid Sea Ice Motion Vectors. Version 3. Boulder, CO, USA: National Snow and Ice Data Center*, 2016, doi: [10.5067/O57VAIT2AYYY](https://doi.org/10.5067/O57VAIT2AYYY).
- [41] R. Kwok, "Annual cycles of multiyear sea ice coverage of the arctic Ocean: 1999–2003," *J. Geophys. Res.: Atmos.*, vol. 109, pp. 227–251, 2004.
- [42] S. Szanyi, J. Lukovich, D. Barber, and G. Haller, "Persistent artifacts in the NSIDC ice motion data set and their implications for analysis," *Geophys. Res. Lett.*, vol. 43, pp. 1–8, 2016.
- [43] R. Kwok, "Annual cycles of multiyear sea ice coverage of the Arctic Ocean: 1999–2003," *J. Geophys. Res.: Oceans (1978–2012)*, vol. 109, pp. 1–13, 2004.
- [44] N. Ivanova, O. M. Johannessen, L. T. Pedersen, and R. T. Tonboe, "Retrieval of Arctic sea ice parameters by satellite passive microwave sensors: A comparison of eleven sea ice concentration algorithms," *IEEE Trans. Geosci. Remote Sens.*, vol. 52, no. 11, pp. 7233–7246, Nov. 2014.
- [45] M. Zygmuntowska *et al.*, "Uncertainties in Arctic sea ice thickness and volume: New estimates and implications for trends," *Cryosphere Discuss.*, vol. 7, pp. 5051–5095, 2014.
- [46] R. L. Tilling *et al.*, "Increased Arctic sea ice volume after anomalously low melting in 2013," *Nature Geosci.*, vol. 8, pp. 643–646, 2015.
- [47] H. Melling, P. H. Johnston, and D. A. Riedel, "Measurements of the underside topography of sea ice by moored subsea sonar," *J. Atmos. Ocean. Technol.*, vol. 12, pp. 589–602, 1995.
- [48] N. Kurtz *et al.*, "Sea ice thickness, freeboard, and snow depth products from operation IceBridge airborne data," *Cryosphere*, vol. 7, pp. 1035–1056, 2013.
- [49] N. Kurtz, M. S. Studinger, J. Harbeck, V. Onana, and D. Yi, *IceBridge LA Sea Ice Freeboard, Snow Depth, and Thickness, Version 1*. Boulder, CO, USA: NASA National Snow and Ice Data Center Distributed Active Archive Center, 2015.
- [50] NSIDC. 2015. [Online]. Available: https://nsidc.org/data/docs/daac/icebridge/evaluation_products/sea-icefreeboard-snowdepth-thickness-quicklook-index.html. Accessed on: October 17, 2015.
- [51] R. L. Tilling, A. Ridout, and A. Shepherd "Near-real-time Arctic sea ice thickness and volume from CryoSat-2," *Cryosphere*, vol. 12, pp. 1–15, 2016.
- [52] R. Ricker *et al.*, "A weekly arctic sea-ice thickness data record from merged cryosat-2 and SMOS satellite data," *Cryosphere Discuss.*, pp. 1–27, 2017.
- [53] R. L. Tilling, A. Ridout, and A. Shepherd "Estimating arctic sea ice thickness and volume using CryoSat-2 radar altimeter data," *Adv. Space Res.*, 2017, (In press).
- [54] R. Ricker *et al.*, "Sensitivity of CryoSat-2 Arctic sea-ice freeboard and thickness on radar-waveform interpretation," *Cryosphere*, vol. 8, pp. 1607–1622, 2014.
- [55] J. Stroeve, T. Markus, L. Boisvert, J. Miller, and A. Barrett, "Changes in Arctic melt season and implications for sea ice loss," *Geophys. Res. Lett.*, vol. 41, pp. 1216–1225, 2014.
- [56] M. C. Serreze and J. Stroeve, "Arctic sea ice trends, variability and implications for seasonal ice forecasting," *Philos. Trans. R. Soc. A*, vol. 373, p. 20140159, 2015.



Haibo Bi received the Ph.D. degree in cartography and geographic information systems from the Institute of Remote Sensing Applications, Chinese Academy of Sciences, Beijing, China, in 2013.

Between 2014 and 2015, he completed his Post-doctoral Research at the Institute of Oceanology, Chinese Academy of Sciences, Qingdao, China, where he became a Fellow in 2015. His current research interests include the investigation of Arctic sea ice kinetics, sea ice mass balance, and using remote sensing tools.



Jinlun Zhang received the Ph.D. degree in oceanography from Dartmouth College, Hanover, NH, USA, in 1993.

He joined the Polar Science Center of the University of Washington, Seattle, WA, USA, in 1994. He is interested in quantifying and understanding climate change in the Polar Regions. He is currently engaged in investigating the properties of polar ice-ocean systems by developing large-scale sea ice and ocean models such as the Pan-arctic Ice-Ocean Modeling and Assimilation System (PIOMAS), the Global Ice-

Ocean Modeling and Assimilation System (GIOMAS), and the Marginal Ice Zone Modeling and Assimilation System (MIZMAS). He is also involved in studying the impact of changes in sea ice on marine planktonic ecosystems by developing biophysical models such as the coupled Biology-Ice-Ocean Modeling and Assimilation System (BIOMAS). He has developed efficient sea ice dynamics models that are particularly useful for stable, high-resolution modeling. His current research interests include developing next-generation sea ice models that capture anisotropic nature of ice dynamics/mechanics and explicitly simulate both ice thickness distribution and floe size distribution jointly.



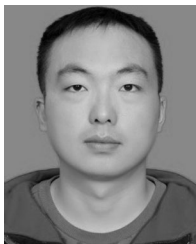
Yunhe Wang received the Bachelor's degree in Shandong University of Technology, Zibo, China, in 2015. He is currently working toward the Ph.D. degree with the Institute of Oceanology, Chinese Academy of Sciences, Qingdao, China.

His current research interests include variability of sea ice concentration and connections with climate factors in the Arctic Ocean and the effects of cloud forcing on sea ice in the Southern Ocean.



Zehua Zhang received the Ph.D. degree in marine geology from the Institute of Oceanology, Chinese Academy of Sciences, Qingdao, China, in 2017.

He is currently with the Chinese Academy of Sciences. His current research interests include sea ice dynamics.



Yi Zhang received the Ph.D. degree in marine geology from the Institute of Oceanology, Chinese Academy of Sciences (IOCAS), Qingdao, China, in 2018.

He plans to continue his research as a Post-doctoral Research Fellow with IOCAS. His current interests of research focus on sea ice and sedimentary environment.



Haijun Huang received the Ph.D. degree in marine geology from the Institute of Oceanology, Chinese Academy of Sciences, Qingdao, China, in 1984.

He is currently with the Institute of Oceanology, Chinese Academy of Sciences. His current research interests include examining the relationship between coastal environment and onshore maritime dynamics with field measurements and satellite remotely sensed imagery.



Min Fu received the Ph.D. degree in marine geology from the Institute of Oceanology, Chinese Academy of Sciences, Qingdao, China, in 2013.

She is currently engaged in contributing to the climate changes and Arctic sea ice changes. She now is a member of National Forecasting Center, Beijing, China, where she leads a study associated with Arctic sea ice drift observations from different platforms.



Xiuli Xu received the M.S. degree in environmental science from Qingdao University of Science and Technology, Qingdao, China, in 2010.

She is currently a Staff Member at the First Institute of Oceanography, State Oceanic Administration (SOA), Qingdao. She is engaged in a research program related to Arctic sea ice extent change and variability, led by Dr. Haibo Bi. Her current research interests include processing and analysis of spaceborne observational data.